Article

Supplementary Material: Y-Shaped Demultiplexer Photonic Circuits Based on Detuned Stubs: Application to Radiofrequency Domain

Abdelkader Mouadili [1], **Soufyane Khattou [2]**, **Madiha Amrani[2]**, **El Houssaine El Boudouti[2]**, **Noureddine Fettouhi[3]**, **Abdelkrim Talbi [4]**, **Abdellatif Akjouj [5]** and **Bahram Djafari-Rouhani [5]***

1. Laboratoire Matériaux, Energie et Contrôle Système, Département de Physique, Faculté des Sciences et Techniques de Mohammedia, Université Hassan II, 28806 Casablanca, Morocco; Abdelkader.mouadili@etu.univh2c.ma
2. Laboratoire de Physique de la Matière et du Rayonnement, Département de Physique, Faculté des Sciences, Université Mohammed I, 60000 Oujda, Morocco; s.khattou@ump.ac.ma (S.K.); m1.amrani@ump.ac.ma (M.A.); e.elboudouti@ump.ac.ma (E.H.E.B.)
3. ESMAR, Département de Physique, Faculté des Sciences, Université Mohammed V, 10000 Rabat, Morocco; n.fettouhi@um5r.ac.ma
4. Université Lille, CNRS, Centrale Lille, Université Polytechnique Hauts-de-France, UMR 8520-IEMN, LIA LICS, F-59000 Lille, France; abdelkrim.talbi@univ-lille.fr
5. Département de Physique, Université de Lille, Institut d'Electronique, de Microélectronique et de Nanotechnologie (IEMN), UMR CNRS 8520, 59655 Villeneuve d'Ascq, France; abdellatif.akjouj@univ-lille.fr
* Correspondence: bahram.djafari-rouhani@univ-lille.fr

The Supplementary material provides the details of analytical calculations of the inverse of the Green's function of the U-shaped demultiplexer which enables us to derive the transmission and reflection coefficients through the system (Section S1). This device presents different possibilities of demultiplexing such as Fano resonances on both outputs (Fano-Fano), EIT resonances on both outputs (EIT-EIT) as well as Fano resonance on one output and EIT resonances on the other output (Fano-EIT). These two latter cases are discussed in Section S2 and Section S3 respectively. In Section S4, we present the analytical calculation of the interface Green's function of the finite photonic circuit in presence of a defect cavity. In Section S5, we give preliminary results about the transposition of the results presented in this paper for demultiplexers operating in radiofrequency domain to plasmonic demultiplexer based on metal-insulator-metal (MIM) nanometric waveguides operating in terahertz domain.

S1. Transmission and reflection coefficients through the U-shaped demultiplexer

We consider a homogeneous isotropic infinite dielectric medium "i" characterized by an impedance Z_i and a dielectric permittivity ε_i. The Green's function between two points x and x' of the material is given by:

$$G_i(x, x') = -jZ \frac{e^{-jk|x-x'|}}{2\omega}, \tag{S.1}$$

where k is the wavevector given by the relation

$$k = \frac{\omega \sqrt{\varepsilon_i}}{c}. \tag{S.2}$$

ω is the pulsation, c the speed of light in vacuum and $j = \sqrt{-1}$.

In order to calculate the transmission and reflection coefficients through the U-shaped demultiplexer (Fig. 1), we need the inverse of the Green's function of the whole structure [1]. This latter can be obtained by the knowledge of the inverse Green's function of the elementary constituents, namely, the Green's functions of finite segments and stubs of

length d_i, $(i = 0, 0', 1, 2, 3, 4, 5, 6)$, and a semi-infinite guide. The boundary conditions at the ends of all waveguides are H = 0 (perfect magnetic conductor). The segment of length d_i $(i = 0, 0', 5, 6)$ is delimited by two surfaces located at $x = 0$ and $x = d_i$ (Fig. 1). These surface elements can be written in the form of a (2×2) matrix $g_i(MM)$, within the interface space $M = \{0, +d_i\}$. The inverse of this matrix takes the following form [1,2]:

$$g_i^{-1}(MM) = \begin{pmatrix} -\frac{\omega C_i}{Z_i S_i} & \frac{\omega}{Z_i S_i} \\ \frac{\omega}{Z_i S_i} & -\frac{\omega C_i}{Z_i S_i} \end{pmatrix} \tag{S.3}$$

The inverse of the Green's surface function of the resonators grafted at sites $\{2\}$, $\{3\}$, $\{4\}$ and $\{5\}$ are given respectively by $g_i^{-1}(2,2) = g_i^{-1}(3,3) = g_i^{-1}(4,4) = g_i^{-1}(5,5) = -\omega S_i / Z_i C_i$, where $C_i = \cos(kd_i)$, $S_i = \sin(kd_i)$ $(i = 1, 2, 3, 4)$ and $k = \omega \frac{\sqrt{\varepsilon_d}}{c}$ is the wavevector. The inverse of the surface Green's functions of the three semi-infinite waveguides which surround the whole structure are given by $g_s^{-1}(1,1) = g_s^{-1}(3,3) = g_s^{-1}(5,5) = j\omega / Z_s$, where Z_s is the characteristic impedance of the semi-infinite cable labeled 's'. In the following, we assume that all the wires are standard coaxial cables with the same characteristic impedance and permittivity (i.e., $Z_0 = Z_1 = Z_2 = Z_3 = Z_4 = Z_5 = Z_6 = Z_s = Z = 50\Omega$ and $\varepsilon_0 = \varepsilon_1 = \varepsilon_2 = \varepsilon_3 = \varepsilon_4 = \varepsilon_5 = \varepsilon_6 = \varepsilon_s = \varepsilon = 2.3$). The expression giving the inverse of Green's function of the whole system given in Fig. 1 can be obtained from a linear superposition of the inverse Green's functions of the above constituents in the interface space $M = \{1, 2, 3, 4, 5\}$, namely

$$g^{-1}(MM) = \frac{-\omega}{Z} \begin{pmatrix} \frac{C_5}{S_5} + \frac{C_6}{S_6} - j & -\frac{1}{S_5} & 0 & -\frac{1}{S_6} & 0 \\ -\frac{1}{S_5} & \frac{C_5}{S_5} + \frac{C_0}{S_0} + \frac{S_1}{C_1} & -\frac{1}{S_0} & 0 & 0 \\ 0 & -\frac{1}{S_0} & \frac{C_0}{S_0} + \frac{S_2}{C_2} - j & 0 & 0 \\ -\frac{1}{S_6} & 0 & 0 & \frac{C_6}{S_6} + \frac{C'_0}{S'_0} + \frac{S_3}{C_3} & -\frac{1}{S'_0} \\ 0 & 0 & 0 & -\frac{1}{S'_0} & \frac{C'_0}{S'_0} + \frac{S_4}{C_4} - j \end{pmatrix}. \tag{S.4}$$

Let us take an incident wave $U(x) = e^{-jkx}$ launched in the left semi-infinite guide of the demultiplexer (Fig. 1). The amplitude of transmitted waves in the first and second output waveguides t_1 and t_2 as well as the reflection coefficient r in the input waveguide are given by $t_1 = (2j\omega/Z)g(1,3)$, $t_2 = (2j\omega/Z)g(1,5)$, and $r = -1 - (2j\omega/Z)g(1,1)$ respectively. By inverting analytically the matrix in Eq. (S.4) and truncating the elements $g(1,3)$, $g(1,5)$ and $g(1,1)$, one can obtain the expressions of t_1, t_2 and r.

S2. Demultiplexer based on EIT-EIT resonances

In addition to Fano-Fano resonances presented in section II of the manuscript, the U-shaped resonator is capable to present also EIT-EIT resonances on both outputs. For this purpose, we have to take the lengths of the two stubs d_1 and d_2 in the first output different and slightly shifted from $\frac{d_0}{2}$ (i.e., $d_1 = \frac{d_0}{2} - \frac{\delta}{2}$ and $d_2 = \frac{d_0}{2} + \frac{\delta}{2}$). Also, in the second output the lengths of the two stubs d_3 and d_4 should be taken slightly different from $\frac{d'_0}{2}$ (i.e., $d_3 = \frac{d'_0}{2} - \frac{\delta}{2}$ and $d_2 = \frac{d'_0}{2} + \frac{\delta}{2}$).

To perform a complete transmission in the first output $(T_1 = 1)$, we have to cancel both the transmission in the second output and the reflection (i.e., $T_2 = R = 0$). By following the same analytical demonstrations discussed in section II, vanishing both T_2 and R at the same frequency, requires that $C_3 = 0$ (or $C_4 = 0$) and $C_5 = 0$. The position of the EIT resonance in the first output is fixed by $\sin(kd_0) = 0$. Likewise, to realize $T_2 = 1$ (i.e., $T_1 = R = 0$), we should satisfy $C_1 = 0$ (or $C_2 = 0$) and $C_6 = 0$. Also, the position of the EIT resonance in the second output is fixed by $\sin(kd'_0) = 0$. Therefore, in order to reach an efficient demultiplexing in both outputs, the eight lengths d_0, d'_0, d_1, d_2, d_3, d_4, d_5 and d_6 must respect the following conditions:

$$d_1 = \frac{d_0}{2} - \frac{\delta}{2}, \tag{S.5}$$

$$d_2 = \frac{d_0}{2} + \frac{\delta}{2}, \tag{S.6}$$

$$d_3 = \frac{d_0}{2}, \tag{S.7}$$

$$d_4 = \frac{d_0}{2} + \delta, \tag{S.8}$$

$$d_5 = \frac{d_0}{2} + \frac{\delta}{2}, \tag{S.9}$$

$$d_6 = \frac{d_0}{2}, \tag{S.10}$$

$$d_0' = d_0 + \delta, \tag{S.11}$$

where $\delta = d_2 - d_1$ represents the detuning between the two stubs of lengths d_1 and d_2. In what follows, we fix the length of the segment $d_0 = d_1 + d_2 = 1$ m which fixes the position of the EIT resonance along the first output.

In order to illustrate the above analytical results, we present in Fig. S1 the variation of the transmissions T_1 and T_2 along the two outputs and the reflection along the input for different values of δ. Figure S1 shows that when the transmission in the first output (blue line) reaches unity ($T_1 = 1$), the transmission in the second output (red line) and the reflection (black line) vanish (i.e., $T_2 = R = 0$). In the same way, when the transmission in the second output reaches unity ($T_2 = 1$), the transmission in the first output and the reflection cancel together (i.e., $T_1 = R = 0$). The two filtered resonances have an EIT-like shape, i.e., a resonance squeezed between two transmission zeros induced by the two resonators. As mentioned before, the resonance in the first output always falls at the same dimensionless frequency ($\Omega = \pi$) for all values of δ, its width increases by increasing δ and vanishes for $\delta = 0$ (Fig. S1). In addition, the shape and width of the EIT resonances are slightly affected when δ becomes negative (i.e., when permuting both stubs 1 and 2). The frequency and width of the resonance in the second output strongly depends on δ in comparison with the resonance in the first output. Indeed, as the first EIT resonance has two transmission zeros around $\Omega = \pi$, the position of the second EIT resonance falls below $\Omega = \pi$ for $\delta > 0$ on the left-hand side of the EIT resonance in output 1, it crosses the first EIT resonance as δ decreases (Fig. S1 (b)) and then reappears above $\Omega = \pi$ for $\delta < 0$ on the right-hand side of the first EIT resonance (Figs. S1 (d), (e)). For $\delta = 0$, the two EIT resonances fall at the same dimensionless frequency giving rise to a BIC state which is characterized by a zero-width (i.e., infinite quality factor) as shown in Fig. S1 (c).
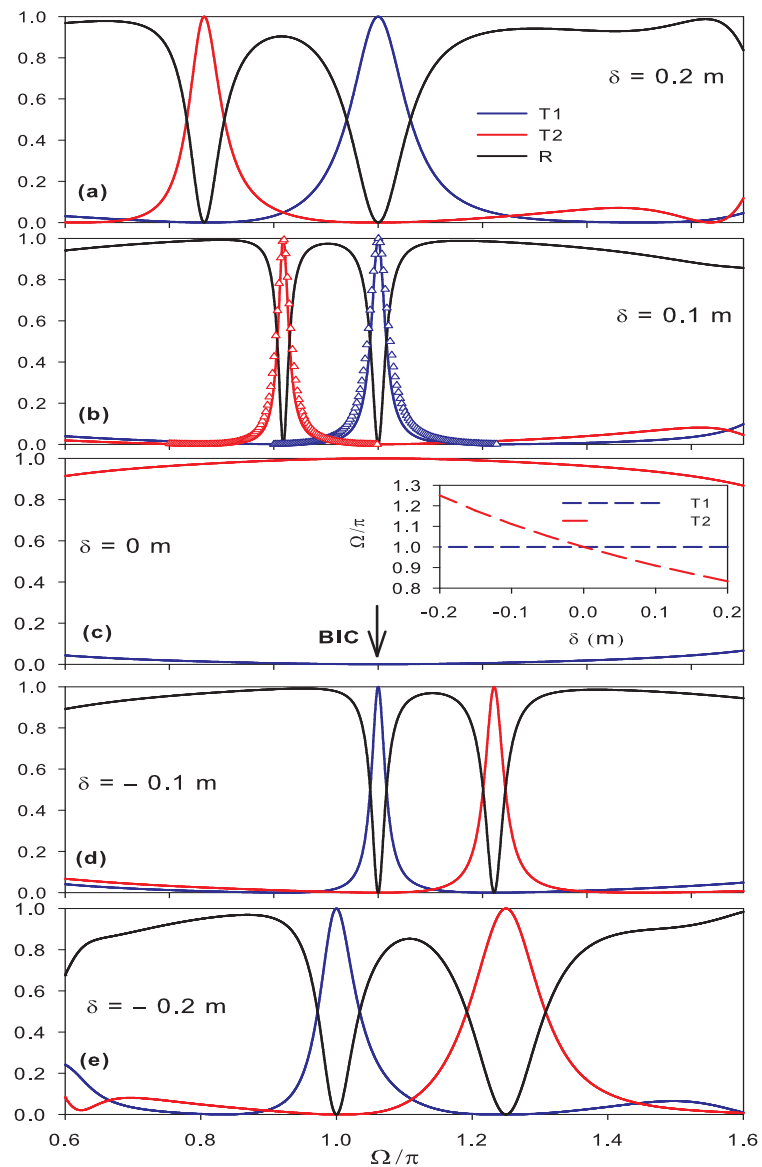
Figure S1. Variation of the intensity of the transmitted signal in output 1 (blue lines), output 2 (red lines) and the reflected signal in the input of the demultiplexer (black lines) as function of the dimensionless frequency Ω/π ($\Omega = \omega d_0 \sqrt{\varepsilon_d}/c$). The lengths of the resonators are given as function of δ where $\delta = d_2 - d_1$ and $d_0 = 1$ m is the length of the segment that separates the segments d_1 and d_2. The other lengths are chosen to satisfy Eqs. (S.5)– (S.11). Red and blue triangles in Fig. (b) correspond to the fitted results obtained by the EIT formula in Eq. (S.12). The inset in Fig. (c) shows the variation of the frequencies of the two EIT resonances as a function of δ.

The full width at half maximum (or equivalently the quality factor) of the EIT resonances strongly depends on the detuning δ between the lengths of the stubs (Eqs. (S.5)– (S.11)). We can notice that the resonances fall side by side and that their widths decrease when δ decreases. Also, when δ changes sign (i.e., when permuting the two stubs of lengths d_1 and d_2), the position of the first EIT resonance remains constant at the same frequency, whereas the second resonance appears below $\Omega = \pi$ as shown in the inset of Fig. S1 (c). Both resonances cross each other at $\delta = 0$.

In order to show that the resonances in the two output lines in Fig. S1 (b) are of EIT type which are characterized by a symmetric shape, the latter should follow the EIT formula, namely [3]

$$T = B \frac{(\omega - \omega_r + q_1\Gamma)^2(\omega - \omega_r + q_2\Gamma)^2}{(\omega - \omega_r)^2 + \Gamma^2}, \tag{S.12}$$

where $B = \frac{1}{q_1 q_2 \Gamma}$. q_1 and q_2 are the Fano parameters and Γ is the width of the EIT resonance lying at ω_r. We can notice a very good agreement between the exact results of the transmission in the first output (blue line) and the fitted results (blue triangles) obtained from Eq. (S.12) for $\delta = 0.1$ m with $\omega_r = \pi$, $q_1 = 10$, $q_2 = -12$ and $\Gamma = 0.035\pi$. Similar results are found for the second transmission coefficient T_2 (red curves) with $\omega_r = 2.86$, $q_1 = 10$, $q_2 = -12$ and $\Gamma = 0.025\pi$. ω_r and Γ are given in units of $d_0\sqrt{\varepsilon_d}/c$.

Figure S2 presents an experimental verification of the simulation results presented in Fig. S1. In the experiment we have chosen the appropriate lengths of the waveguides to obtain EIT resonances on both outputs in the case where $\delta = -0.2$ m, which fixes the lengths of the different waveguides according to Eqs. (S.5)– (S.11) as follows: $d_1 = 0.6$ m, $d_2 = 0.4$ m, $d_0 = 1$ m, $d_3 = 0.5$ m, $d_4 = 0.3$ m, $d_5 = 0.4$ m, $d_6 = 0.5$ m and $d_0' = 0.8$ m. The experiment shows that the absorption in the cables affects the amplitude of the resonances, which do not exceed 60%. However, we note that when the transmission is maximal in one output line, both the transmission in the second output line and the reflection in the input get close to zero. In Fig. S2, the crosstalk rate between the two outputs for the frequency 97.11 MHz is about -30.9 dB. This rate becomes about -34.81 dB for the frequency 122.61 MHz.
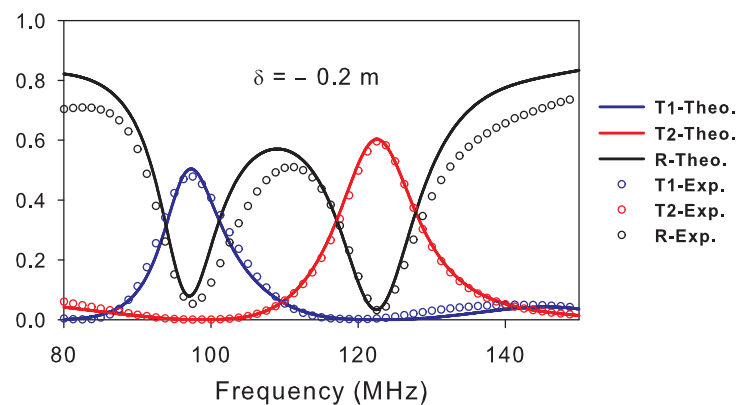
Figure S2. Theoretical (continuous lines) and experimental (open circles) transmission and reflection coefficients as a function of the frequency along the ports 1 (blue curves) and 2 (red curves). The reflection coefficient is sketched by the black curves for $\delta = -0.2$ m. The lengths of the different cables are chosen according to Eqs. (S.5)– (S.11).

S3. Demultiplexer based on Fano-EIT resonances

The third possibility of demultiplexing that can be presented by the U-shaped resonator is based on EIT resonance in one output and Fano resonance in the second output. This case represents a mixed filtering. By using the same analytical calculations as in section II, in order to obtain an EIT resonance in output 1 one should satisfy $C_3 = 0$ (or $C_4 = 0$), $\sin(kd_0) = 0$ and $C_6 = 0$. In the same way, to obtain a Fano type resonance in the output 2, one should verify $C_1 = 0$ (or $C_2 = 0$), $\sin(k(d_0' + \delta)) = 0$ and $C_5 = 0$. Therefore, the lengths of all waveguides must respect the following equations:

$$d_1 = \frac{d_0}{2} - \frac{\delta}{2}, \tag{S.13}$$

$$d_2 = \frac{d_0}{2} + \frac{\delta}{2}, \tag{S.14}$$

$$d_3 = d_4 = \frac{d_0}{2}, \tag{S.15}$$

$$d_5 = \frac{d_0}{2} + \frac{\delta}{2}, \tag{S.16}$$

$$d_6 = \frac{d_0}{2}, \tag{S.17}$$

$$d_0' = d_0 + 2\delta, \tag{S.18}$$

where $\delta = d_2 - d_1$.

Based on the conditions given by Eqs. (S.13)–(S.18), we plot in Fig. S3 the transmission and reflection coefficients as a function of the dimensionless frequency in the case of a hybrid demultiplexer based on EIT and Fano resonances. Figure S3 gives the simulation results in the case of lossless system for several cases of δ, the blue curve shows the transmission through the first output and the red curve shows the transmission through the second output and the black curve gives the reflection at the input of the demultiplexer. The curves of Fig. S3 show that the filtered resonance on the output 1 is of EIT type and the filtered resonance on the output 2 is of Fano type. The position of the EIT resonance remains constant at the same frequency since we have fixed the length of d_0, whereas the change in δ causes a change in the position of the Fano resonance and the width of the two resonances. In particular for $\delta = 0$, the two resonances fall at the same dimensionless frequency giving rise to a BIC state (Fig. S3 (c)).
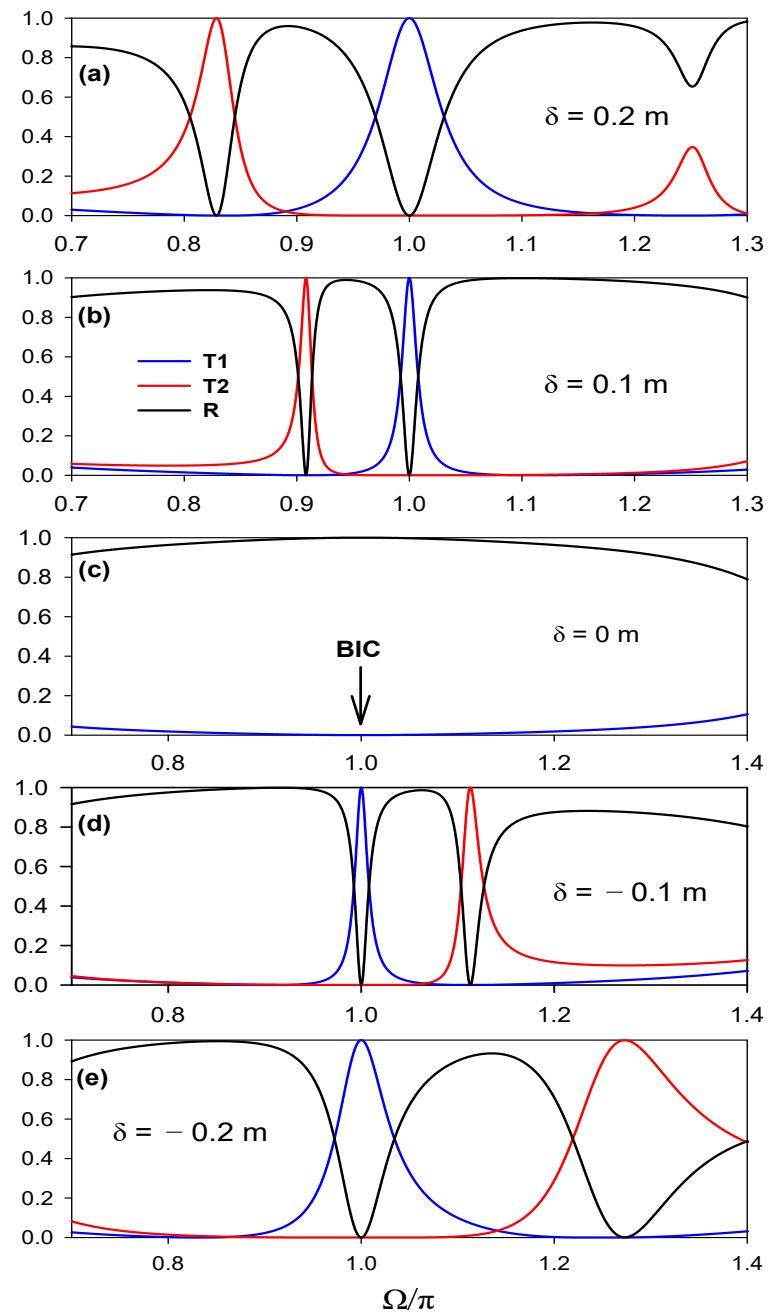
Figure S3. Variation of the intensity of the transmitted signal in output 1 (blue lines), output 2 (red lines) and the reflected signal at the input of the demultiplexer (black lines) versus the dimensionless frequency Ω/π ($\Omega = \frac{\omega d_0 \sqrt{\varepsilon_d}}{c}$). The lengths of the resonators are given as function of δ and d_0 is fixed at $d_0 = 1$ m. The other lengths are chosen according to Eqs. (S.13)– (S.18).

An experimental verification of this case is presented in Fig. S4, the lengths of the stubs are chosen according to Eqs. (S.13)– (S.18), the transmissions of the two resonances do not reach unity due to the loss in the cables. The theoretical results are presented by solid lines and the experimental results are given by open circles. Both results show a good agreement. In Fig. S4, the crosstalk rate between the two outputs for the frequency 97.11 MHz is about -61.20 dB. This rate becomes about -23.65 dB for the frequency 125.04 MHz.
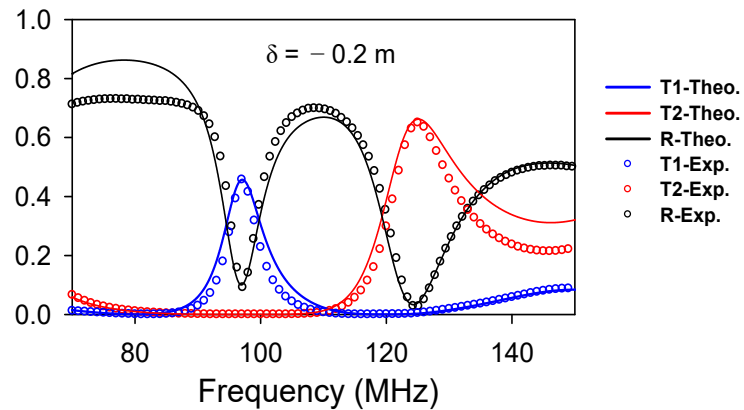
Figure S4. Theoretical (continuous lines) and experimental (open circles) transmission and reflection coefficients as a function of the frequency for $\delta = -0.2$ m along the ports 1 (blue curves) and 2 (red curves). The reflection coefficient is sketched by the black curves.

S4. Interface Green's function of the finite photonic crystal with defect

The photonic circuit is formed of an infinite number of segments of length d_1 (Fig. S5 (a)). Each segment has two free surfaces. The interface domain consists of all connection points between the segments. Each connection point (called site) is defined by an integer n. A resonator of length d_2 is grafted onto each site. The position x in a cell between sites n and $n+1$ is represented by the pair (n, x) where x is a local coordinate such as $0 \leq x \leq d_1$ and d_1 in this case represents the period of the structure.
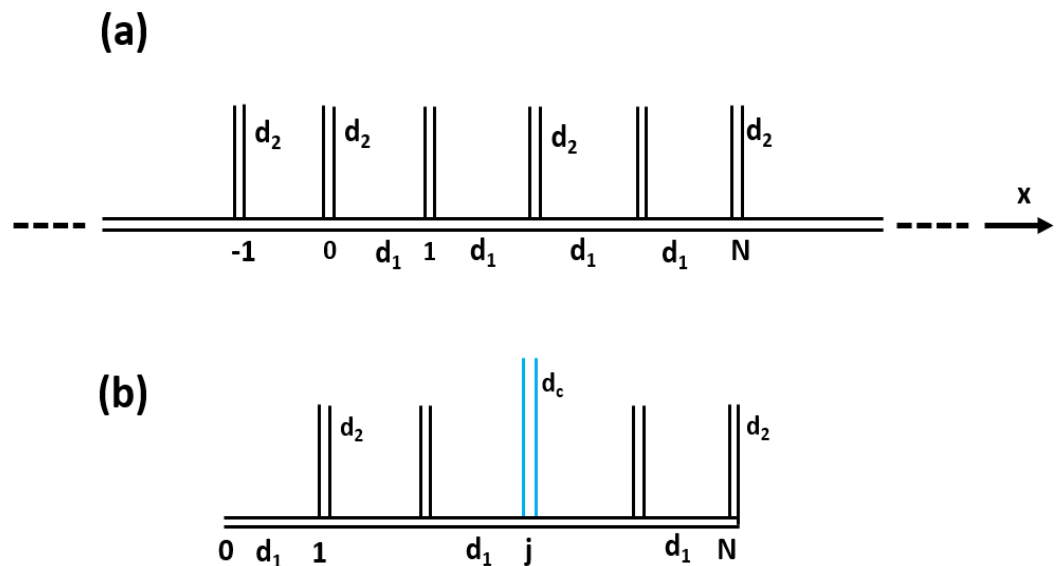
Figure S5. Schematic representation of the infinite comb structure (a) and finite comb structure composed of N stubs of lengths d_2 (b). The stubs are separated by segments of length d_1.

In order to calculate the Green's function of the infinite photonic crystal (Fig. S5 (a)), we need first the Green's function of each constituent, namely the Green's function of a segment of length d_1 and the Green's function of a resonator of length d_2. These surface elements are noted respectively $g_1(M_1, M_1)$, which is a matrix (2×2) in the space of interfaces $M_1 = \{0, d_1\}$ and $g_2(0, 0)$. The inverse of the matrix $g_1(M_1 M_1)$ is given by [4]:

$$g_1^{-1}(M_1 M_1) = \begin{pmatrix} -\dfrac{\omega C_1}{Z S_1} & \dfrac{\omega}{Z S_1} \\ \dfrac{\omega}{Z S_1} & -\dfrac{\omega C_1}{Z S_1} \end{pmatrix}, \tag{S.19}$$

while $g_2(i,i)$ depends on the choice of the boundary conditions at the end of the resonators, i.e., E = 0 (i.e., vanishing electric field) or H = 0 (i.e., vanishing magnetic field). In this work, we only consider the case where H = 0. In this case, the inverse of this quantity in the interface space $M = \{i\}$ is given by [2]:

$$g_2^{-1}(i,i) = -\frac{\omega S_2}{ZC_2},$$

(S.20)

where C_i and S_i are defined as

$$C_i = \cos(kd_i) \quad and \quad S_i = \sin(kd_i) \quad (i = 1, 2).$$

(S.21)

In the interface space of the infinite comb structure, the inverse of the Green's function $g^{-1}(MM)$ is an infinite tridiagonal matrix formed by the superposition of the elements $g_i^{-1}(M_i, M_i)(i = 1, 2)$. This matrix can be written as follows:

$$g^{-1}(MM) = \begin{pmatrix} \ddots & \ddots & \ddots & & & \\ & v & w & v & & \\ & & v & w & v & \\ & & & v & w & v \\ & & & & \ddots & \ddots & \ddots \end{pmatrix},$$

(S.22)

where

$$w = -\frac{2\omega C_1}{ZS_1} - \frac{\omega S_2}{ZC_2}$$

(S.23)

and

$$v = \frac{\omega}{ZS_1}.$$

(S.24)

From the above matrix (Eq. (S.22)), one can derive the dispersion relation of the periodic comb structure, namely [4]

$$\cos(kd_1) = C_1 - \frac{1}{2}\frac{S_1 S_2}{C_2}.$$

(S.25)

Now, we consider a finite photonic circuit composed of N sites with a cavity (stub defect) (Fig. S5 (b)). We present the details of the calculation of the Green's function at both extremities of the finite structure with defect.

Let us use a cleavage operator which consists of removing the segment located between the sites $n = -1$ and $n = 0$ on one side and $n = N$ and $n = N + 1$ on the other side in order to create a finite system (Fig. S5(b)). Then, we remove the stub of length d_2 on the site $n = 0$ and replace the stub of length d_2 on the site j by a stub of length d_c. Consequently, the disturbed interface space is composed of $M_s = \{-1, 0, j, N, N+1\}$.

In this case, the perturbation operator $V(M_s M_s)$ is given by:

$$V(M_s M_s) = \frac{\omega}{Z}\begin{pmatrix} \frac{C_1}{S_1} & \frac{-1}{S_1} & 0 & 0 & 0 \\ \frac{-1}{S_1} & \frac{C_1}{S_1} + \frac{S_2}{C_2} & 0 & 0 & 0 \\ 0 & 0 & \frac{S_2}{C_2} - \frac{S_c}{C_c} & 0 & 0 \\ 0 & 0 & 0 & \frac{C_1}{S_1} & -\frac{1}{S_1} \\ 0 & 0 & 0 & \frac{-1}{S_1} & \frac{C_1}{S_1} \end{pmatrix}.$$

(S.26)

The knowledge of the elements of the response function in the space of the interfaces of the infinite comb structure (Eq. (S.22)) and those of the perturbation operator $V(M_s M_s)$ (Eq. (S.26)), allows us to deduce the elements of the response function of the finite structure necessary for the calculation of the transmission and reflection coefficients. The operator $\Delta(M_s M_s)$ is given by [1]

$$\Delta(M_s M_s) = I(M_s M_s) + V(M_s M_s)g(M_s M_s) \tag{S.27}$$

where

$$g(M_s M_s) = \frac{S_1}{F_1}\frac{t}{t^2-1}\begin{pmatrix} 1 & t & t^j & t^N & t^{N+1} \\ t & 1 & t^{j-1} & t^{N-1} & t^N \\ t^j & t^{j-1} & 1 & t^{N-j} & t^{N+1-j} \\ t^N & t^{N-1} & t^{N-j} & 1 & t \\ t^{N+1} & t^N & t^{N+1-j} & t & 1 \end{pmatrix}. \tag{S.28}$$

After calculating the operator $\Delta(M_s M_s)$, we write this operator in the interface space $M_0 = \{0, 1, j, N\}$. The response function of the finite comb structure in the interface space M_0 is given by the following equation:

$$d(M_0 M_0) = g(M_0 M_0)\Delta^{-1}(M_0 M_0). \tag{S.29}$$

From Eq. (S.29), we deduce the truncated matrix $d_{tr}(M'_0 M'_0)$ in the interface space $M'_0 = \{0, N\}$ which represents the two extremities of the finite structure. The inverse of this matrix can be written as follows

$$d_{tr}^{-1}(M'_0 M'_0) = \begin{pmatrix} A' & B \\ B & A \end{pmatrix}. \tag{S.30}$$

This latter matrix associated to the finite photonic circuit (Fig. S5(b)) serves as a starting point (see Eq. (14)) to establish the Green's function of the Y-shaped demultiplexer based on two photonic circuits (Eq. (15)). It is sufficient to connect these systems to semi-infinite waveguides and then to deduce the transmission and reflection coefficients (Eqs. (16)-(18)).

S5. Transposition to plasmonic demultiplexer based on metal-insulator-metal waveguides

As mentioned before, the results presented in this paper can be transported to plasmonic demultiplexers based on metal-insulator-metal (MIM) nano-waveguides and operating in the telecommunication domain around 1.55 μm [5]. In this section, we give a preliminary result of a plasmonic demultiplexer based on periodic circuits with different cavities on each output as shown in Fig. S6 (a). All MIM waveguides have the same width $d = 50$ nm (Fig. S6 (a)). The waveguides are filled with air, while the surrounding metal is made of silver. Figures S6 (b) and (c) represent the transmission spectra through two output waveguides of the plasmonic demultiplexer without and with cavities respectively. Each MIM waveguide is formed of a finite plasmonic circuit composed of three resonators of lengths $d_2 = 260$ nm separated by a waveguide of length $d_1 = 520$nm. In Fig S6 (b), we give the transmission spectrum along the two outputs where the two plasmonic outputs are chosen without defects (i.e., $d_{c1} = d_{c2} = d_2 = 260$ nm). One can see clearly the existence of a large gap around 120-280 THz. Thus, by detuning appropriately the length of the two cavities, we can filter two closed frequencies inside the gaps. However, in order to select two plasmonic modes along each output, the two cavity defects should be taken slightly different from each other such as $d_{c1} = 520$ nm and $d_{c2} = 380$ nm. Figure S6 (c) gives the transmission along the first (blue curves) and the second (red curves) outputs. One can see two filtered resonances inside the gap along each output. These results are similar to those found in Fig. 9 of the main manuscript in the radio-frequency domain. The simulation results are obtained by using comsol Multiphysics software.
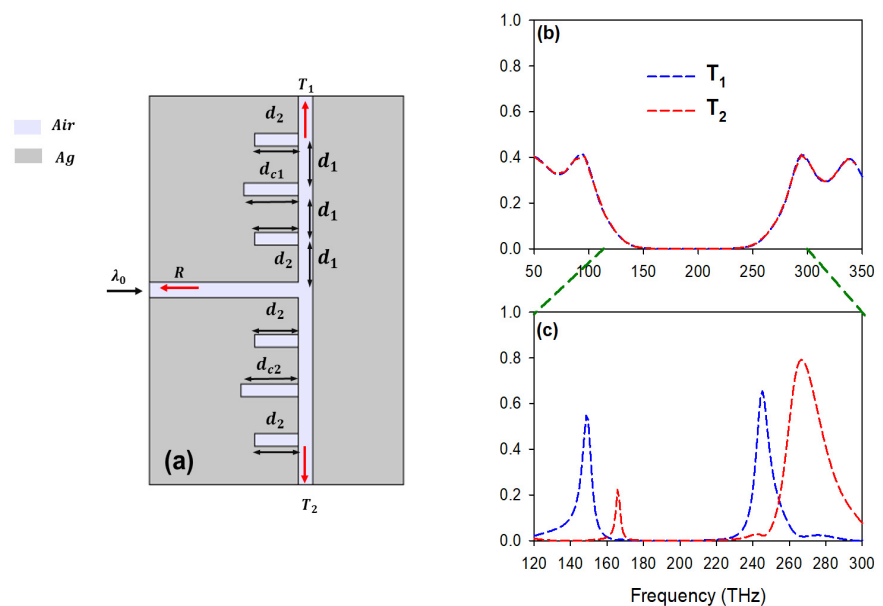
Figure S6. (a) Schematic representation of the plasmonic demultiplexer with one input and two outputs. Each output consists of a finite plasmonic structure composed of (N=3) resonators with specific resonator defect. The resonators are of lengths d_2, the segments that connect the resonators are of lengths d_1 and the defects are of lengths d_{c1} on the output 1 and d_{c2} on the output 2. (b) Transmission coefficient through the two outputs of the demultiplexer: (b) $d_{c1} = d_{c2} = d_2 = 260$nm (without defect) and $d_1 = 520$nm, (c) $d_{c1} = 520$nm (blue curve) and $d_{c2} = 380$nm (red curve), while $d_1 = 520$nm.

References

1. Dobrzynski, L.; Akjouj, A.; Boudouti, E.H.E.; Lêveque, G.; Al-Wahsh, H.; Pennec, Y.; Ghouila-Houri, C.; Talbi, A.; Djafari-Rouhani, B.; Jin, Y. *Photonics*; Elsevier: Amsterdam, The Netherlands, 2020.
2. Vasseur, J.O.; Akjouj, A.; Dobrzynski, L.; Djafari-Rouhani, B.; Boudouti, E.H.E. Photon, electron, magnon, phonon and plasmon mono-mode circuits. *Surf. Sci. Rep.* **2004**, *54*, 1.
3. Fleischhauer, M.; Imamoglu, A.; Marangos, J.P. Electromagnetically induced transparency: Optics in coherent media. *Rev. Mod. Phys.* **2005**, *77*, 633.
4. Djafari-Rouhani, B.; Boudouti, E.H.E.; Akjouj, A.; Dobrzynski, L.; Vasseur, J.O.; Mir, A.; Fettouhi, N; Zemmouri, J. Surface states in one-dimensional photonic band gap structures. *Vac.* **2001**, *63*, 177.
5. Amrani, M.; Khattou, S.; Noual, A.; Boudouti, E.H.E.; Djafari-Rouhani, B. Plasmonic Demultiplexer Based on Induced Transparency Resonances: Analytical and Numerical Study. *Lect. Notes Electr. Eng.* **2021**, *681*, 239.